JGP Journal of General Physiology

COMMENTARY

Myofilament Function 2022

Variants of the myosin interacting-heads motif

Raúl Padrón[1], Debabrata Dutta[1], and Roger Craig[1]

Under relaxing conditions, the two heads of myosin II interact with each other and with the proximal part (S2) of the myosin tail, establishing the interacting-heads motif (IHM), found in myosin molecules and thick filaments of muscle and nonmuscle cells. The IHM is normally thought of as a single, unique structure, but there are several variants. In the simplest ("canonical") IHM, occurring in most relaxed thick filaments and in heavy meromyosin, the interacting heads bend back and interact with S2, and the motif lies parallel to the filament surface. In one variant, occurring in insect indirect flight muscle, there is no S2–head interaction and the motif is perpendicular to the filament. In a second variant, found in smooth and nonmuscle single myosin molecules in their inhibited (10S) conformation, S2 is shifted ∼20 Å from the canonical form and the tail folds twice and wraps around the interacting heads. These molecule and filament IHM variants have important energetic and pathophysiological consequences. (1) The canonical motif, with S2–head interaction, correlates with the super-relaxed (SRX) state of myosin. The absence of S2–head interaction in insects may account for the lower stability of this IHM and apparent absence of SRX in indirect flight muscle, contributing to the quick initiation of flight in insects. (2) The ∼20 Å shift of S2 in 10S myosin molecules means that S2–head interactions are different from those in the canonical IHM. This variant therefore cannot be used to analyze the impact of myosin mutations on S2–head interactions that occur in filaments, as has been proposed. It can be used, instead, to analyze the structural impact of mutations in smooth and nonmuscle myosin.

The canonical IHM

The myosin II molecule has two heads and a long tail (Fig. 1 B b; Geeves and Holmes, 2005). Under relaxing conditions, the heads can interact with each other through a head–head interaction first found in 2-D crystals of smooth muscle heavy meromyosin (HMM) and myosin in the off-state (Wendt et al., 2001; Liu et al., 2003), creating a blocked head (BH) and free head (FH; Fig. 1 A). Cryo-EM studies later showed that this interaction also occurs in native, relaxed thick filaments of tarantula (Woodhead et al., 2005), and revealed an additional interaction, brought about by folding back of the heads onto the tail, in which the BH mesa (Spudich, 2015) interacts with S2. These two basic, intramolecular interactions (BH–FH and BH–S2) were later also demonstrated in single molecules of smooth muscle HMM (Burgess et al., 2007), and define the interacting-heads motif (IHM; Fig. 1 A; Woodhead et al., 2005; Alamo et al., 2008, 2017a). We propose the term "canonical" to describe this basic IHM structure, as it is the simplest and most common IHM, occurring in isolated HMM molecules (therefore independent of any interaction with the distal portion of the tail [light meromyosin] or with other proteins), and in numerous thick filament types (*Limulus* [Zhao et al., 2009], scorpion [Pinto et al., 2012], and scallop [Woodhead et al., 2013] muscle; mouse [Zoghbi et al., 2008], human [Al-Khayat et al., 2013], and zebrafish [Gonzalez-Sola et al., 2014] cardiac muscle; Fig. 1 C), and schistosome smooth muscle (Sulbaran et al., 2015); reviewed in Alamo et al. (2018). While interaction of S2 with the BH in filaments has only been directly observed in tarantula (Fig. 1 C c), it is assumed to occur in these other species, and to be an integral component of the canonical IHM (Fig. 1 C; Blankenfeldt et al., 2006; Alamo et al., 2017b, 2018; Nag et al., 2017; Woodhead and Craig, 2020).

Two variants of the IHM

Two exceptions to the canonical IHM structure have been described. One occurs in thick filaments of the indirect flight muscles of insects ("insect variant"; Fig. 1 D), specialized for the rapid contraction–relaxation cycles that power insect flight (Hu et al., 2016). The other ("10S variant"; Fig. 1 B) is found in single molecules of smooth and nonmuscle myosin II, in which the tail is folded to produce a compact, inhibited conformation with a 10S sedimentation coefficient, specialized as an inactive storage

[1]Division of Cell Biology and Imaging, Department of Radiology, University of Massachusetts Chan Medical School, Worcester, MA.

Correspondence to Raul Padron: raul.padron@umassmed.edu

This work is part of a special issue on Myofilament Function 2022.

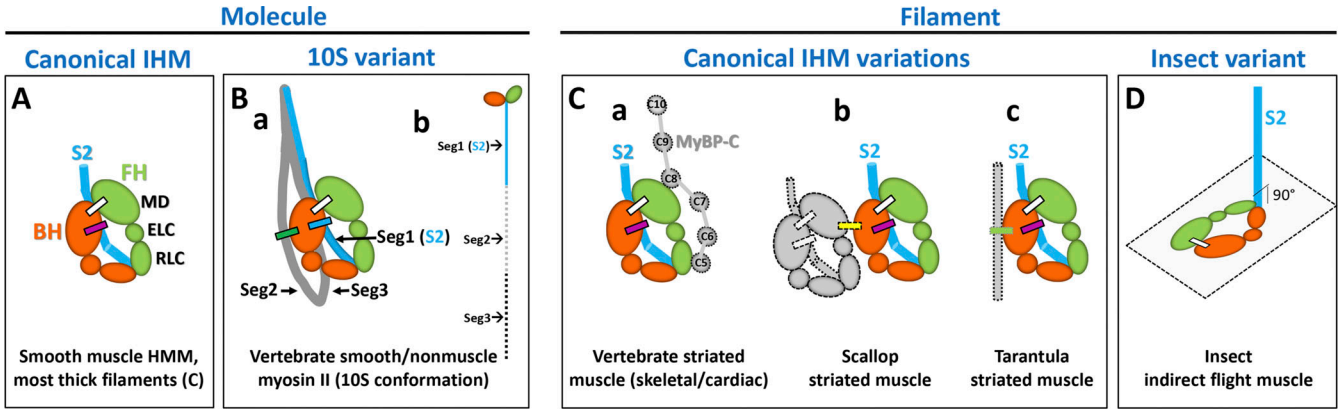

Figure 1. **The canonical myosin IHM and its variants. (A)** Canonical IHM present in smooth muscle HMM and most thick filaments (see C), showing the blocked and free heads (BH, orange; FH, green), with BH–FH interaction (white bar) and BH–S2 interaction (purple bar). MD, myosin II motor domain; RLC, myosin II regulatory light chain; ELC, myosin II essential light chain. **(B)** 10S variant present in isolated vertebrate smooth and nonmuscle myosin II molecules in their inhibited, folded conformation, with interactions between BH and FH (white bar), BH and tail segments 1 and 3 (blue bar), and the BH and tail segment 2 (green bar). Inset b shows myosin molecule with tail extended. **(C)** IHM variations in thick filaments, where the canonical IHM placed in a thick filament environment may undergo additional (intermolecular) interactions: (a) vertebrate striated, showing hypothetical interaction with MyBP-C; (b) scallop striated, with additional interactions between other IHMs in the same crown (yellow bar); and (c) tarantula striated, with additional interaction (green bar) between BH and S2 from IHM in the axially adjacent crown. IHMs in all these variations are parallel to the filament surface. **(D)** IHM variant in *Lethocerus* indirect flight muscle thick filaments (insect variant), where IHM is perpendicular to S2 and the filament surface, showing BH–FH interactions (white bar) but no interaction with S2 (blue).

molecule that can be activated for motile function when required (Heissler and Sellers, 2016). This 10S single molecule variant appears to be ubiquitous across the evolutionary tree, from sponges to humans (Jung et al., 2008; Lee et al., 2018).

What structural differences distinguish these variants from the canonical IHM? In the insect filament variant, there are two distinct modifications. There is no interaction of S2 with either head, and the motif is perpendicular to the filament axis, in contrast to the parallel arrangement in the canonical structure found in all other filaments (Fig. 1 D, cf. Fig. 1 C; Hu et al., 2016). In the 10S molecule variant, the tail bends twice, creating three segments, which wrap around the interacting heads (Fig. 1 B). Within the IHM (S2 and the two heads), S2 (segment 1) is shifted off the mesa, to a point ∼20 Å closer to the tip of the BH compared with the canonical structure (Fig. 2, B and C). For the remainder of the molecule outside the IHM, segment 2 passes around the BH, and segment 3 bends back onto the BH, taking the place of S2 in the canonical IHM (Fig. 2 A). These different locations of S2 on the BH are due to the different courses that it takes as it leaves the junction of the heads. In the canonical IHM, S2 runs diagonally across the hole formed between the two heads, then bends to travel over the BH mesa (Fig. 1 A). In the 10S variant, S2 follows a straight course and crosses the BH close to the tip of the BH motor, ∼20 Å distant from S2 in the canonical IHM (Fig. 2 A; Yang et al., 2020; Scarff et al., 2020; Heissler et al., 2021). Comparison of the tarantula filament (canonical) IHM, in which the S2 densities have been clearly detected in the low-resolution cryo-EM 3-D maps, and the 10S variant (known at high-resolution) reveals two further differences. When the tarantula IHM and molecule variant are superimposed by alignment of their BHs, their FHs are less well aligned. This local mismatch suggests significant conformational differences of the corresponding heads in the two structures. In addition, in the tarantula IHM, S2 crosses the BH within 3 Å of the mesa surface, suggesting substantial interaction, while in its ∼20 Å–displaced position in the 10S variant, it hovers ∼10 Å above the BH, implying minimal interaction (Fig. 2, B and C, bottom).

Functional and energetic differences between IHM variants

These differences in S2 shape and interactions have important functional consequences, as the residues of the BH involved in the BH–S2 interaction in the canonical IHM and the insect filament and 10S molecule variants are different, with implications for both muscle energetics (ATP saving) and structural understanding of disease pathogenesis.

The intramolecular interactions that constrain head motions and block binding sites in the canonical IHM are thought to be the main structural basis of the slow myosin ATP turnover rate, termed super-relaxation (SRX; Fig. 1 A), that occurs in vertebrate skeletal (Stewart et al., 2010) and cardiac (Hooijman et al., 2011) muscle (Fig. 1 C a; reviewed in Craig and Padron [2022]). Additional intermolecular "locking" interactions in tarantula (Fig. 1 C c) and scallop (Fig. 1 C b) may further constrain BH ATPase activity, possibly accounting for an even slower ATP turnover rate, termed hyper-relaxation (HRX), in these species (Vibert and Craig, 1983; Cooke, 2011; Naber et al., 2011; Alamo et al., 2016; reviewed in Craig and Padron [2022]). We refer to these as "variations" of the canonical IHM (i.e., the IHM is similar to the canonical structure, but its properties are modified by these additional intermolecular interactions). Vertebrate filaments only exhibit SRX. Potential interactions of canonical IHMs with MyBP-C and titin (Fig. 1 C a) therefore do not appear to produce additional locking interactions, but may be involved with fine-tuning the SRX fraction or activation from the SRX state (McNamara et al., 2016; McNamara et al., 2019; Nelson

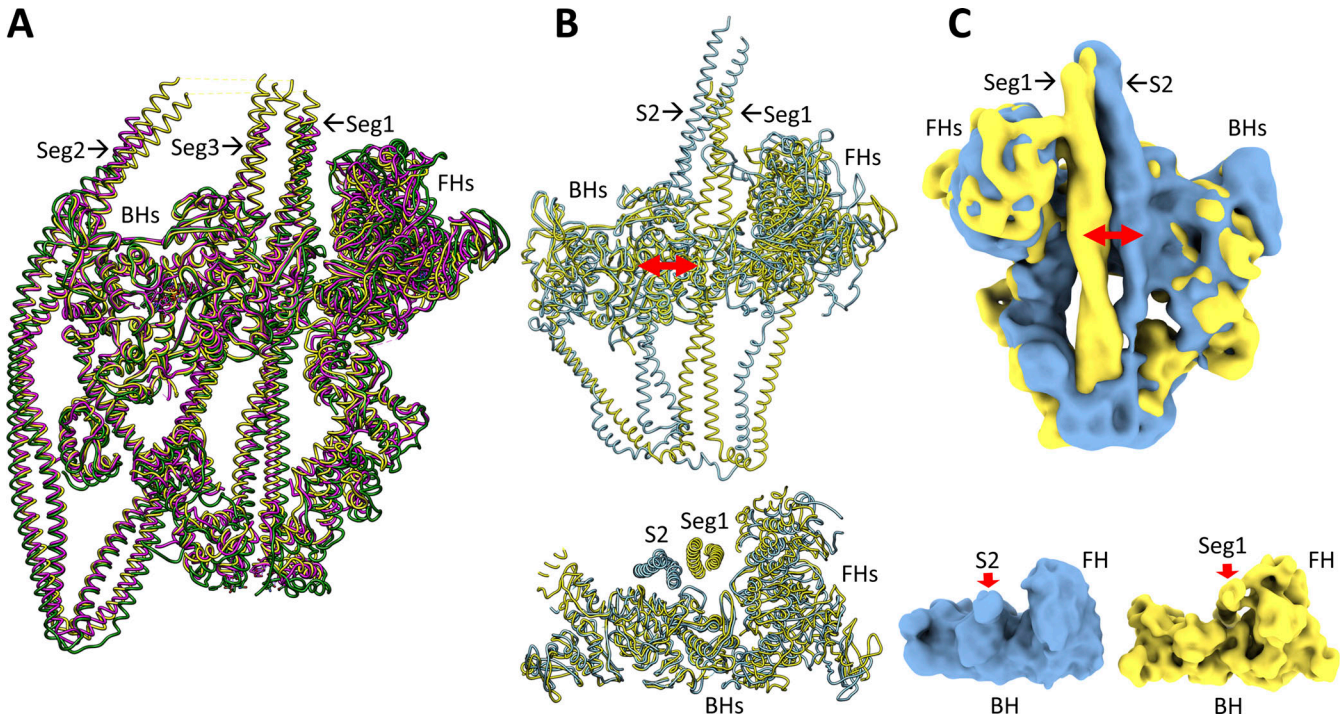

Figure 2. **20 Å difference in position of segment 1 of the 10S IHM variant compared with S2 in the canonical IHM. (A)** PDB structures for the 10S molecule variant (6XE9 [yellow], 6Z47 [purple], 7MF3 [green]) show similar locations for the three tail segments (Segs1–3). **(B)** Top: Comparison of 10S variant (PDB accession no. 6XE9 [yellow]) with tarantula canonical IHM (PDB accession no. 3JBH [blue]) with light chains removed for simplicity, showing Seg1 of the molecule shifted ∼20 Å closer to the tip of the BH than S2 in the filament (red double arrow). Bottom: Horizontal slice of top view, rotated 90° to show Seg1 of the molecule ∼10 Å above the BH (yellow), implying little or no interaction, while S2 in the tarantula canonical IHM (blue) is within 3 Å of the BH mesa and could interact. **(C)** Top: Superposition of the cryo-EM densities of the 10S variant (EMD accesison no. EMD-22145; low-pass filtered to 10 Å resolution, yellow) and the ∼12 Å resolution tarantula filament canonical IHM (blue), showing a ∼22 Å S2–Seg1 shift (red double arrow). This view is rotated 180° around a vertical axis compared with A and B to best reveal S2/Seg1, on the rear of the IHM. Bottom: Individual 3-D map densities showing that Seg1 (red arrow) does not interact with the BH in the molecule variant (yellow), while S2 (red arrow) of the tarantula canonical IHM (blue) docks on the BH mesa. A and B were made with UCSF Chimera, C was made with UCSF ChimeraX.

et al., 2020; reviewed in Craig and Padron [2022]). A locking interaction similar to that in tarantula also occurs in the 10S IHM (Yang et al., 2020; Scarff et al., 2020; Heissler et al., 2021), between the BH and segment 2 of the tail (Figs. 1 B and 2 A), possibly constraining the BH ATPase in this variant and giving rise to HRX in the molecule as well (Cross et al., 1988; Craig and Padron, 2022).

BH–S2 interaction is absent from insect (*Lethocerus*) indirect flight muscle thick filaments (Hu et al., 2016). This interaction is thought to initiate head folding in the canonical IHM (Alamo et al., 2016) and its absence in *Lethocerus* may account for the lower stability of this IHM, implied by the weak head density in thick filament 3-D reconstructions from this species (Hu et al., 2016). If the IHM underlies SRX (Craig and Padron, 2022), this would predict little or no SRX for this class of animal (Fig. 1 D). Thick filaments of *Drosophila* flight muscle show little head ordering and appear not to form an IHM at all (Daneshparvar et al., 2020), consistent with the absence of SRX in *Drosophila* muscle (Ochala, J., personal communication), the only species where SRX has not been found. The absence of SRX, and weak or no IHM in insect indirect flight muscle, may be a specialization to keep myosin heads fully unlocked, for instant interaction with actin, allowing for rapid take off and escape from danger (predators, swatting hands) or pursuit of prey.

Mapping disease mutations onto IHM variants

A homology model of the vertebrate cardiac IHM, based on the 20 Å-resolution cryo-EM structure of the tarantula filament IHM, was used successfully to map the location of mutations causing hypertrophic cardiomyopathy (HCM) and dilated cardiomyopathy (DCM; Alamo et al., 2017b; Nag et al., 2017). A key finding was that many HCM and DCM mutations clustered in the BH–FH and BH–S2 interfaces, suggesting that disruption or stabilization of the IHM by these mutations might underlie the respective hyper- or hypo-contractile phenotype of these diseases. To fully understand the impact of these mutations, an atomic structure of the human cardiac thick filament IHM is required. Despite crystallization of HMM of squid muscle and the achievement of near-atomic (∼5 Å) resolution in the x-ray diffraction pattern, no IHM crystallographic structure has yet been solved (O'Neall-Hennessey et al., 2013), and efforts to obtain tarantula HMM crystals of sufficient size were unsuccessful. In addition, mammalian cardiac thick filament structure has been solved only to 30–40 Å resolution (by negative stain 3-D reconstruction; Zoghbi et al., 2008; Al-Khayat et al., 2013), due to weakness of the IHM interactions, their pseudo-helical arrangement, and the presence of myosin binding protein C (MyBP-C) and titin, all of which hinder structural analysis. Similar and more complex issues inhibit cryo-EM studies, and

no cryo-EM structure of cardiac thick filaments has yet been reported.

The achievement of near-atomic resolution for the 10S IHM molecule variant (Yang et al., 2020; Scarff et al., 2020; Heissler et al., 2021; Fig. 2 A) opened new hope for analyzing the structural impact of HCM and DCM mutations on IHM stability and interactions. These molecule IHM variants are the only available near-atomic PDB structures reported so far for an IHM. It was proposed that the improved, near-atomic resolution of the 10S variant may "be invaluable as a model for understanding mutations in striated muscle myosins, such as those in β-cardiac myosin that result in hypertrophic cardiomyopathy" (Scarff et al., 2020) and "will facilitate future basic and translational research efforts to describe how mutations destabilize or dysregulate the IHM and lead to HCM and to exploit previously unidentified inter- and intramolecular interfaces for the development of mechanism-based therapeutics for HCM" (Heissler et al., 2021). However, as already noted (Yang et al., 2020), S2 in the 10S variant is shifted ∼20 Å laterally from its position in the canonical IHM (assumed to be the structure present in the cardiac thick filament), and is also at a distance (∼10 Å) from the surface of the BH mesa that would weaken or eliminate any interaction (see above). Thus, analysis of cardiac mutations occurring in the BH–S2 interface is not possible with the 10S molecule variant. Further, analysis of other key mutations (e.g., in the BH–FH interface) requires the assumption that these IHM interactions are the same in the canonical IHM and the 10S variant, which we pointed out earlier may not be the case. Solving the structure of the human cardiac IHM thus remains an urgent need.

Despite these drawbacks, the molecule variant is precisely the structure required to analyze disease-causing mutations in smooth and nonmuscle myosin (Yang et al., 2020). These myosins have essential roles in numerous cellular functions (smooth muscle contraction, nonmuscle motility, cytokinesis), and multiple diseases are linked to mutations in their heavy chains, including breast and prostate cancer, blood diseases, and smooth muscle dysfunction (Ma and Adelstein, 2014; Abrams et al., 2016). These mutations map mainly to regions of head–tail and tail–tail interaction in the folded myosin structure, supporting the key role played by this conformation in normal cell function (Yang et al., 2020). Thus, in both the canonical IHM and 10S variant, mutations involved in key intramolecular interaction interfaces may be crucial in the causation of skeletal, cardiac, smooth muscle, and nonmuscle cell diseases.

Is HMM a canonical IHM or a 10S molecule variant: Can it be used to analyze HCM and DCM mutations?

HMM is a fragment of myosin used to elucidate myosin function in solution, where a soluble molecule is required. It consists of the two heads attached to the first segment (S2) of the myosin tail, and is made by proteolytic digestion of tissue-prepared myosin (Margossian and Lowey, 1982). Similar molecules, but with shorter tails (25 or 15 heptads of α-helix) can be prepared using a protein expression system (Anderson et al., 2018), which also enables the effects of mutations to be studied (Anderson et al., 2018; Rasicci et al., 2022 *Preprint*). Can these truncated molecules be used to elucidate the structural impact of mutations on cardiac myosin function? This depends on whether HMM forms the (canonical) IHM present in filaments (Fig. 1 C a), where mutational effects are expressed in vivo, or possibly the IHM present in the molecule (10S) variant (Fig. 1 B), which might be expected for an isolated molecule such as HMM. A recent study suggests that cardiac HMM forms the canonical IHM (Fig. 1 A), not the 10S variant (Fig. 1 B), and is thus appropriate for mutational analysis (Rasicci et al., 2022 *Preprint*). The mutation E525K in the myosin mesa causes DCM, characterized by inhibition of contractile activity. This mutation enhances SRX in a 15-heptad HMM of cardiac myosin, while also increasing formation of a compact ("closed") structure according to FRET solution observations; direct EM imaging demonstrates that these compact molecules have a folded-back IHM structure whose numbers increase with the mutation. In the folded-back, canonical IHM, E525 on the BH mesa is next to a ring of negative charge on S2: charge reversal at E525, from negative to positive, would therefore be expected to stabilize the folded back structure through increased attraction of S2 for the BH, as observed (Rasicci et al., 2022 *Preprint*). Thus, S2 position in the canonical IHM directly explains this stabilization, whereas the 10S variant, in which S2 is 20 Å distant, would not. We conclude that the IHM in single HMM molecules is canonical—similar to that in cardiac filaments—and therefore appropriate for analyzing the impact of mutations on living cardiac muscle. What is needed now is its structure. One approach to this question has been modeling of a 25-heptad HMM structure based on low angle x-ray scattering (Gollapudi et al., 2021). This suggests that cardiac HMM in solution may not have a single structure, but can form other closed conformations (this would be consistent with the weak intramolecular interactions on which the IHM is based). However, the precise nature of these conformations remains to be determined.

Work will remain even after the single molecule cardiac IHM structure is solved. IHMs in vertebrate thick filaments are arranged along pseudo-helical tracks, with different interactions *between* IHMs at different levels of heads spaced 13–15 nm apart in each helix (Zoghbi et al., 2008; Al-Khayat et al., 2013). It will be important to determine whether any of the documented cardiomyopathy mutations occur in these *inter*molecular interactions, which can be analyzed only in filaments, as well as the *intra*molecular interactions that can be elucidated using the HMM structure. Additional intermolecular interactions may also occur between IHMs and MyBP-C, titin and the light meromyosin tails forming the filament backbone (Zoghbi et al., 2008; Al-Khayat et al., 2013), possibly leading to further IHM variations (Fig. 1 C a) in different vertebrate striated muscles (cardiac, fast and slow skeletal) due to different myosin and MyBP-C isoforms, which may contribute to differing properties of SRX in these diverse muscle types (Stewart et al., 2010; Hooijman et al., 2011; reviewed in Craig and Padron [2022]). Analysis of these possibilities will require a high-resolution cryo-EM structure of the human cardiac thick filament, which has yet to be achieved. The atomic structure not only of the cardiac IHM in solution, but also in the thick filament, where it may interact with MyBP-C and titin, remains a pressing need,

currently impeded by the mixed populations of IHM (SRX) and non-IHM (DRX) myosins and complex distribution of non-myosin components along the vertebrate thick filament.

Acknowledgments

Henk L. Granzier served as editor.

We thank Dr. Julien Ochala for sharing information concerning the absence of SRX in insect indirect flight muscle, and Dr. Prince Tiwari and Mr. Vu Nguyen for discussions.

This work was supported by National Institutes of Health grants AR072036, HL139883, and HL164560. UCSF Chimera is supported by National Institutes of Health grant P41 RR001081 (Pettersen et al., 2004). Molecular graphics and analyses were performed with UCSF ChimeraX, developed by the Resource for Biocomputing, Visualization, and Informatics at the University of California, San Francisco, with support from National Institutes of Health R01-GM129325 and the Office of Cyber Infrastructure and Computational Biology, National Institute of Allergy and Infectious Diseases (Pettersen et al., 2021).

The authors declare no competing financial interests.

References

Abrams, J., Z. Einhorn, C. Seiler, A.B. Zong, H.L. Sweeney, and M. Pack. 2016. Graded effects of unregulated smooth muscle myosin on intestinal architecture, intestinal motility and vascular function in zebrafish. *Dis. Model. Mech.* 9:529–540. https://doi.org/10.1242/dmm.023309

Al-Khayat, H.A., R.W. Kensler, J.M. Squire, S.B. Marston, and E.P. Morris. 2013. Atomic model of the human cardiac muscle myosin filament. *Proc. Natl. Acad. Sci. U.S.A.* 110:318–323. https://doi.org/10.1073/pnas.1212708110

Alamo, L., J.S. Ware, A. Pinto, R.E. Gillilan, J.G. Seidman, C.E. Seidman, and R. Padron. 2017b. Effects of myosin variants on interacting-heads motif explain distinct hypertrophic and dilated cardiomyopathy phenotypes. *Elife*. 6. e24634. https://doi.org/10.7554/eLife.24634

Alamo, L., A. Pinto, G. Sulbaran, J. Mavarez, and R. Padron. 2018. Lessons from a tarantula: New insights into myosin interacting-heads motif evolution and its implications on disease. *Biophys. Rev.* 10:1465–1477. https://doi.org/10.1007/s12551-017-0292-4

Alamo, L., D. Qi, W. Wriggers, A. Pinto, J. Zhu, A. Bilbao, R.E. Gillilan, S. Hu, and R. Padron. 2016. Conserved intramolecular interactions maintain myosin interacting-heads motifs explaining tarantula muscle super-relaxed state structural basis. *J. Mol. Biol.* 428:1142–1164. https://doi.org/10.1016/j.jmb.2016.01.027

Alamo, L., N. Koubassova, A. Pinto, R. Gillilan, A. Tsaturyan, and R. Padron. 2017a. Lessons from a tarantula: New insights into muscle thick filament and myosin interacting-heads motif structure and function. *Biophys. Rev.* 9:461–480. https://doi.org/10.1007/s12551-017-0295-1

Alamo, L., W. Wriggers, A. Pinto, F. Bártoli, L. Salazar, F.-Q. Zhao, R. Craig, and R. Padrón. 2008. Three-dimensional reconstruction of tarantula myosin filaments suggests how phosphorylation may regulate myosin activity. *J. Mol. Biol.* 384:780–797. https://doi.org/10.1016/j.jmb.2008.10.013

Anderson, R.L., D.V. Trivedi, S.S. Sarkar, M. Henze, W. Ma, H. Gong, C.S. Rogers, J.M. Gorham, F.L. Wong, M.M. Morck, et al. 2018. Deciphering the super relaxed state of human beta-cardiac myosin and the mode of action of mavacamten from myosin molecules to muscle fibers. *Proc. Natl. Acad. Sci. U.S.A.* 115:E8143–E8152. https://doi.org/10.1073/pnas.1809540115

Blankenfeldt, W., N.H. Thoma, J.S. Wray, M. Gautel, and I. Schlichting. 2006. Crystal structures of human cardiac beta-myosin II S2-delta provide insight into the functional role of the S2 subfragment. *Proc. Natl. Acad. Sci. U.S.A.* 103:17713–17717. https://doi.org/10.1073/pnas.0606741103

Burgess, S.A., S. Yu, M.L. Walker, R.J. Hawkins, J.M. Chalovich, and P.J. Knight. 2007. Structures of smooth muscle myosin and heavy meromyosin in the folded, shutdown state. *J. Mol. Biol.* 372:1165–1178. https://doi.org/10.1016/j.jmb.2007.07.014

Cooke, R. 2011. The role of the myosin ATPase activity in adaptive thermogenesis by skeletal muscle. *Biophys. Rev.* 3:33–45. https://doi.org/10.1007/s12551-011-0044-9

Craig, R., and R. Padron. 2022. Structural basis of the super- and hyper-relaxed states of myosin II. *J. Gen. Physiol.* 154:e202113012. https://doi.org/10.1085/jgp.202113012

Cross, R.A., A.P. Jackson, S. Citi, J. Kendrick-Jones, and C.R. Bagshaw. 1988. Active site trapping of nucleotide by smooth and non-muscle myosins. *J. Mol. Biol.* 203:173–181. https://doi.org/10.1016/0022-2836(88)90100-3

Daneshparvar, N., D.W. Taylor, T.S. O'Leary, H. Rahmani, F. Abbasiyeganeh, M.J. Previs, and K.A. Taylor. 2020. CryoEM structure of drosophila flight muscle thick filaments at 7 Å resolution. *Life Sci. Alliance*. 3: e202000823. https://doi.org/10.26508/lsa.202000823

Geeves, M.A., and K.C. Holmes. 2005. The molecular mechanism of muscle contraction. *Adv. Protein Chem.* 71:161–193. https://doi.org/10.1016/S0065-3233(04)71005-0

Gollapudi, S.K., W. Ma, S. Chakravarthy, A.C. Combs, N. Sa, S. Langer, T.C. Irving, and S. Nag. 2021. Two classes of myosin inhibitors, para-nitroblebbistatin and mavacamten, stabilize beta-cardiac myosin in different structural and functional states. *J. Mol. Biol.* 433:167295. https://doi.org/10.1016/j.jmb.2021.167295

Gonzalez-Sola, M., H.A. Al-Khayat, M. Behra, and R.W. Kensler. 2014. Zebrafish cardiac muscle thick filaments: Isolation technique and three-dimensional structure. *Biophys. J.* 106:1671–1680. https://doi.org/10.1016/j.bpj.2014.01.050

Heissler, S.M., A.S. Arora, N. Billington, J.R. Sellers, and K. Chinthalapudi. 2021. Cryo-EM structure of the autoinhibited state of myosin-2. *Sci. Adv.* 7:eabk3273. https://doi.org/10.1126/sciadv.abk3273

Heissler, S.M., and J.R. Sellers. 2016. Various themes of myosin regulation. *J. Mol. Biol.* 428:1927–1946. https://doi.org/10.1016/j.jmb.2016.01.022

Hooijman, P., M.A. Stewart, and R. Cooke. 2011. A new state of cardiac myosin with very slow ATP turnover: A potential cardioprotective mechanism in the heart. *Biophys. J.* 100:1969–1976. https://doi.org/10.1016/j.bpj.2011.02.061

Hu, Z., D.W. Taylor, M.K. Reedy, R.J. Edwards, and K.A. Taylor. 2016. Structure of myosin filaments from relaxed *Lethocerus* flight muscle by cryo-EM at 6 A resolution. *Sci. Adv.* 2:e1600058. https://doi.org/10.1126/sciadv.1600058

Jung, H.S., S. Komatsu, M. Ikebe, and R. Craig. 2008. Head-head and head-tail interaction: A general mechanism for switching off myosin II activity in cells. *Mol. Biol. Cell*. 19:3234–3242. https://doi.org/10.1091/mbc.e08-02-0206

Lee, K.H., G. Sulbaran, S. Yang, J.Y. Mun, L. Alamo, A. Pinto, O. Sato, M. Ikebe, X. Liu, E.D. Korn, et al. 2018. Interacting-heads motif has been conserved as a mechanism of myosin II inhibition since before the origin of animals. *Proc. Natl. Acad. Sci. U.S.A.* 115:E1991–E2000. https://doi.org/10.1073/pnas.1715247115

Liu, J., T. Wendt, D. Taylor, and K. Taylor. 2003. Refined model of the 10S conformation of smooth muscle myosin by cryo-electron microscopy 3D image reconstruction. *J. Mol. Biol.* 329:963–972. https://doi.org/10.1016/s0022-2836(03)00516-3

Ma, X., and R.S. Adelstein. 2014. The role of vertebrate nonmuscle myosin II in development and human disease. *Bioarchitecture*. 4:88–102. https://doi.org/10.4161/bioa.29766

Margossian, S.S., and S. Lowey. 1982. Preparation of myosin and its subfragments from rabbit skeletal muscle. *Methods Enzymol.* 85 Pt B:55–71. https://doi.org/10.1016/0076-6879(82)85009-x

McNamara, J.W., R.R. Singh, and S. Sadayappan. 2019. Cardiac myosin binding protein-C phosphorylation regulates the super-relaxed state of myosin. *Proc. Natl. Acad. Sci. U.S.A.* 116:11731–11736. https://doi.org/10.1073/pnas.1821660116

McNamara, J.W., A. Li, N.J. Smith, S. Lal, R.M. Graham, K.B. Kooiker, S.J. van Dijk, C.G.D. Remedios, S.P. Harris, and R. Cooke. 2016. Ablation of cardiac myosin binding protein-C disrupts the super-relaxed state of myosin in murine cardiomyocytes. *J. Mol. Cell. Cardiol.* 94:65–71. https://doi.org/10.1016/j.yjmcc.2016.03.009

Naber, N., R. Cooke, and E. Pate. 2011. Slow myosin ATP turnover in the super-relaxed state in tarantula muscle. *J. Mol. Biol.* 411:943–950. https://doi.org/10.1016/j.jmb.2011.06.051

Nag, S., D.V. Trivedi, S.S. Sarkar, A.S. Adhikari, M.S. Sunitha, S. Sutton, K.M. Ruppel, and J.A. Spudich. 2017. The myosin mesa and the basis of hypercontractility caused by hypertrophic cardiomyopathy mutations. *Nat. Struct. Mol. Biol.* 24:525–533. https://doi.org/10.1038/nsmb.3408

Nelson, S.R., A. Li, S. Beck-Previs, G.G. Kennedy, and D.M. Warshaw. 2020. Imaging ATP consumption in resting skeletal muscle: One molecule at a

time. *Biophys. J.* 119:1050–1055. https://doi.org/10.1016/j.bpj.2020.07.036

O'Neall-Hennessey, E., L. Reshetnikova, V.S. Senthil Kumar, H. Robinson, A.G. Szent-Gyorgyi, and C. Cohen. 2013. Purification, crystallization and preliminary x-ray crystallographic analysis of squid heavy meromyosin. *Acta Crystallogr. Sect. F. Struct. Biol. Cryst. Commun.* 69:248–252. https://doi.org/10.1107/S1744309112049925

Pettersen, E.F., T.D. Goddard, C.C. Huang, E.C. Meng, G.S. Couch, T.I. Croll, J.H. Morris, and T.E. Ferrin. 2021. UCSF ChimeraX: Structure visualization for researchers, educators, and developers. *Protein Sci.* 30:70–82. https://doi.org/10.1002/pro.3943

Pettersen, E.F., T.D. Goddard, C.C. Huang, G.S. Couch, D.M. Greenblatt, E.C. Meng, and T.E. Ferrin. 2004. UCSF Chimera: A visualization system for exploratory research and analysis. *J. Comput. Chem.* 25:1605–1612. https://doi.org/10.1002/jcc.20084

Pinto, A., F. Sanchez, L. Alamo, and R. Padron. 2012. The myosin interacting-heads motif is present in the relaxed thick filament of the striated muscle of scorpion. *J. Struct. Biol.* 180:469–478. https://doi.org/10.1016/j.jsb.2012.08.010

Rasicci, D.V., P. Tiwari, R. Desetty, F. Sadler, S. Sivaramakrishnan, R. Craig, and C.M. Yengo. 2022. Dilated cardiomyopathy mutation E525K in human beta-cardiac myosin stabilizes the interacting heads motif and super-relaxed state of myosin. *bioRxiv* https://doi.org/10.1101/2022.02.18.480995

Scarff, C.A., G. Carrington, D. Casas-Mao, J.M. Chalovich, P.J. Knight, N.A. Ranson, and M. Peckham. 2020. Structure of the shutdown state of myosin-2. *Nature*. 588:515–520. https://doi.org/10.1038/s41586-020-2990-5

Spudich, J.A. 2015. The myosin mesa and a possible unifying hypothesis for the molecular basis of human hypertrophic cardiomyopathy. *Biochem. Soc. Transactions*. 43:64–72. https://doi.org/10.1042/BST20140324

Stewart, M.A., K. Franks-Skiba, S. Chen, and R. Cooke. 2010. Myosin ATP turnover rate is a mechanism involved in thermogenesis in resting skeletal muscle fibers. *Proc. Natl. Acad. Sci. U.S.A.* 107:430–435. https://doi.org/10.1073/pnas.0909468107

Sulbaran, G., L. Alamo, A. Pinto, G. Marquez, F. Mendez, R. Padron, and R. Craig. 2015. An invertebrate smooth muscle with striated muscle myosin filaments. *Proc. Natl. Acad. Sci. U.S.A.* 112:E5660–E5668. https://doi.org/10.1073/pnas.1513439112

Vibert, P., and R. Craig. 1983. Electron microscopy and image analysis of myosin filaments from scallop striated muscle. *J. Mol. Biol.* 165:303–320. https://doi.org/10.1016/s0022-2836(83)80259-9

Wendt, T., D. Taylor, K.M. Trybus, and K. Taylor. 2001. Three-dimensional image reconstruction of dephosphorylated smooth muscle heavy meromyosin reveals asymmetry in the interaction between myosin heads and placement of subfragment 2. *Proc. Natl. Acad. Sci. U.S.A.* 98:4361–4366. https://doi.org/10.1073/pnas.071051098

Woodhead, J.L., and R. Craig. 2020. The mesa trail and the interacting heads motif of myosin II. *Arch. Biochem. Biophys.* 680:108228. https://doi.org/10.1016/j.abb.2019.108228

Woodhead, J.L., F.-Q. Zhao, R. Craig, E.H. Egelman, L. Alamo, and R. Padrón. 2005. Atomic model of a myosin filament in the relaxed state. *Nature*. 436:1195–1199. https://doi.org/10.1038/nature03920

Woodhead, J.L., F.Q. Zhao, and R. Craig. 2013. Structural basis of the relaxed state of a Ca^{2+}-regulated myosin filament and its evolutionary implications. *Proc. Natl. Acad. Sci. U.S.A.* 110:8561–8566. https://doi.org/10.1073/pnas.1218462110

Yang, S., P. Tiwari, K.H. Lee, O. Sato, M. Ikebe, R. Padron, and R. Craig. 2020. Cryo-EM structure of the inhibited (10S) form of myosin II. *Nature*. 588:521–525. https://doi.org/10.1038/s41586-020-3007-0

Zhao, F.Q., R. Craig, and J.L. Woodhead. 2009. Head-head interaction characterizes the relaxed state of *Limulus* muscle myosin filaments. *J. Mol. Biol.* 385:423–431. https://doi.org/10.1016/j.jmb.2008.10.038

Zoghbi, M.E., J.L. Woodhead, R.L. Moss, and R. Craig. 2008. Three-dimensional structure of vertebrate cardiac muscle myosin filaments. *Proc. Natl. Acad. Sci. U.S.A.* 105:2386–2390 https://doi.org/10.1073/pnas.0708912105